



LAWRENCE
LIVERMORE
NATIONAL
LABORATORY

Kinetics of helium bubble formation in nuclear materials

L. L. Bonilla, A. Carpio, J. C. Neu, W. G. Wolfer

November 8, 2005

Physica D

Disclaimer

This document was prepared as an account of work sponsored by an agency of the United States Government. Neither the United States Government nor the University of California nor any of their employees, makes any warranty, express or implied, or assumes any legal liability or responsibility for the accuracy, completeness, or usefulness of any information, apparatus, product, or process disclosed, or represents that its use would not infringe privately owned rights. Reference herein to any specific commercial product, process, or service by trade name, trademark, manufacturer, or otherwise, does not necessarily constitute or imply its endorsement, recommendation, or favoring by the United States Government or the University of California. The views and opinions of authors expressed herein do not necessarily state or reflect those of the United States Government or the University of California, and shall not be used for advertising or product endorsement purposes.

Kinetics of helium bubble formation in nuclear materials

L. L. Bonilla ^{a,*}, A. Carpio ^b, J. C. Neu ^c, W. G. Wolfer ^d,

^a*Grupo de Modelización, Simulación Numérica y Matemática Industrial,
Universidad Carlos III de Madrid, Avenida de la Universidad 30, 28911 Leganés,
Spain*

^b*Departamento de Matemática Aplicada, Universidad Complutense de Madrid,
28040 Madrid, Spain*

^c*Department of Mathematics, Universidad de California at Berkeley, Berkeley, CA
94720; USA*

^d*Lawrence Livermore National Laboratory, Livermore, CA 94550; USA*

Abstract

The formation and growth of helium bubbles due to self-irradiation in plutonium has been modelled by a discrete kinetic equations for the number densities of bubbles having k atoms. Analysis of these equations shows that the bubble size distribution function can be approximated by a composite of: (i) the solution of partial differential equations describing the continuum limit of the theory but corrected to take into account the effects of discreteness, and (ii) a local expansion about the advancing leading edge of the distribution function in size space. Both approximations contribute to the memory term in a close integrodifferential equation for the monomer concentration of single helium atoms. The present theory is compared to the numerical solution of the full kinetic model and to previous approximation of Schaldach and Wolfer involving a truncated system of moment equations.

Key words: discrete kinetic equations, helium bubbles, boundary layers for discrete equations

PACS: 05.20.Dd, 23.60.+e, 05.40.-a

* Corresponding author.

Email addresses: bonilla@ing.uc3m.es (L. L. Bonilla), ana_carpio@mat.ucm.es (A. Carpio), neu@math.berkeley.edu (J. C. Neu), wolfer1@llnl.gov (W. G. Wolfer).

1 Introduction

There are simple kinetic models of irreversible aggregation, in which a cluster with k monomers grows by absorbing one monomer but it cannot decrease in size by shedding part of its mass. An interesting example is the formation and growth of helium bubbles in plutonium alloys as a consequence of alpha decay due to self-irradiation [1,2]. As an alloy ages, there is an initial transient stage during which self-irradiation produces dislocation loops that tend to saturate within approximately two years. The alpha particles created during irradiation become helium atoms. These atoms come to rest at unfilled vacancies generated during their slowing-down process, before they are captured at existing helium bubbles. A helium atom diffuses through the lattice until it finds another helium atom thereby forming a stable dimer or until it finds a helium bubble (a stable cluster with k atoms or, in short, a k -cluster), which absorbs it. Helium bubbles are attached to lattice defects, do not move and do not shed helium atoms because the binding energies of helium to any cluster are extremely high [2]. The following kinetic model based on these observations has been proposed by Schaldach and Wolfer [1]:

$$\dot{\rho}_k = 4\pi D \tilde{c} a_{k-1} \rho_{k-1} - 4\pi D \tilde{c} a_k \rho_k, \quad k \geq 3, \quad (1)$$

$$\dot{\rho}_2 = 8\pi D \tilde{c}^2 a_1 - 4\pi D \tilde{c} a_2 \rho_2, \quad (2)$$

$$\tilde{c} + \sum_{k=2}^{\infty} k \rho_k = \int_0^{\tilde{t}} g(t') dt'. \quad (3)$$

Here $\dot{\rho}_k = d\rho_k/d\tilde{t}$, ρ_k is the number density of k clusters having effective radii a_k (when the center of a monomer comes within distance a_k of the cluster center, it is absorbed), c is the number of monomers per unit volume, D is the diffusion coefficient and $g(\tilde{t})$ is the number of monomers created per unit volume and per unit time. Eq. (3) means that the total number of monomers per unit volume, whether they are in solution or forming part of a k cluster, should equal the time integral of $g(\tilde{t})$. In Equations (1) and (2), k clusters grow by adding one monomer with a rate $4\pi D \tilde{c} a_{k-1}$ (for $k > 2$) to a $k - 1$ cluster, and they do not decay. The mean absorption rate of a monomer by an immobile k cluster (with $k > 1$) is $4\pi D \tilde{c} a_k$, whereas the rate of creation of an immobile dimer by the collision of two mobile monomers is twice this quantity, $8\pi D \tilde{c} a_1$. The absorption rate can be calculated immediately from the concentration field outside a k cluster (i.e., the number of monomers per unit volume in $\tilde{r} > a_k$), $\rho(\tilde{r}, \tilde{t})$. In the process of diffusion-limited adiabatic growth of diluted clusters (such that $a_k^3 \rho_k \ll 1$), $\rho(\tilde{r}, \tilde{t})$ solves the Laplace equation outside $\tilde{r} = a_k$, with $\rho(a_k, \tilde{t}) = 0$, and it takes on the value $\tilde{c}(\tilde{t})$ (the

monomer density in solution) as $\tilde{r} \rightarrow \infty$. Thus

$$\rho(\tilde{r}, \tilde{t}) = \tilde{c}(\tilde{t}) \left(1 - \frac{a_k}{\tilde{r}}\right),$$

for $\tilde{r} > a_k$. The mean absorption rate of monomers by the k cluster is

$$4\pi a_k^2 D \frac{\partial \rho}{\partial \tilde{r}}(a_k, \tilde{t}) = 4\pi D \tilde{c} a_k. \quad (4)$$

The simplest model for the effective radius of a k cluster is based on packing of non-overlapping particles:

$$a_k = a_1 k^{1/3}. \quad (5)$$

It is interesting to observe that a related kinetic system was proposed and solved in 1914 by McKendrick as a model of leucocyte phagocytosis [3]. In McKendrick's model, ρ_k is the density of leucocytes which have ingested k bacteria, and its rate equation is (1) for $k \geq 0$, with a known function of time $\tilde{c}(\tilde{t}) > 0$ and $\rho_{-1} \equiv 0$. McKendrick's solution method involved solving the equation for ρ_0 in terms of $\int \tilde{c} d\tilde{t}$ and solving recursively all other equations for ρ_k as functions of ρ_0 . His method cannot be used to solve the system (1) - (3), but an useful closure of this infinite system to only three differential equations was introduced in [1], and compared to experiments, [1,2].

In this paper, we shall study the solution of the system (1) - (3) starting from an initial condition corresponding to the absence of helium bubbles, i.e.,

$$\tilde{c}(0) = 0, \quad \rho_k(0) = 0, \text{ for } k \geq 2. \quad (6)$$

We shall consider the case of a constant production rate of helium atoms, $g(\tilde{t}) = g \tilde{t}$. Once $\tilde{c}(\tilde{t})$ as been found, the total density of bubbles can be obtained by integrating the equation:

$$\frac{d}{d\tilde{t}} \sum_{k=2}^{\infty} \rho_k = 8\pi D a_1 \tilde{c}^2. \quad (7)$$

Eq. (7) is immediately obtained by adding (2) and (1) (for all $k \geq 3$).

We have found that, after a short transient, the size distribution function becomes a smooth function of k and it is a functional of the monomer concentration. In turn, the monomer concentration satisfies an integrodifferential equation. The size distribution function can be approximated by matched asymptotic expansions. Except for large k , its form is close to the solution

of the hyperbolic equation resulting from replacing derivatives instead of differences in (1), but including corrections due to discreteness. This outer approximation breaks down at large k : it has an unrealistic large peak at a maximum value of k after which the distribution function abruptly falls to zero. If our governing equations were partial differential equations instead of differential-difference equations, we would say that a boundary layer should be inserted to remedy this imperfection. However, the concept of boundary layer is not straightforward for discrete equations. How do we insert a boundary layer approximation to difference equations? The answer to this question lies in the wave front expansion of the Becker-Döring equations some of us introduced in Ref. [4]. This theory yields one equation for the leading edge of the size distribution function and one equation for the distribution function itself near its edge. A solution of the latter written in similarity variables is then matched to the outer approximation and its contribution to the integral terms of the equation for the monomer concentration is calculated. These two steps were not needed for the nucleation calculation in Ref. [4] because there the outer approximation was a constant, size-independent profile and the integral condition was identically satisfied during the nucleation transient. The present overall theory including outer and boundary layer approximations describes quite well the observed numerical simulations of the discrete system of equations.

The rest of the paper is as follows. The nondimensional equations of the model are derived in Section 2. The outer approximation to the size distribution function and the monomer concentration is described in Section 3. The boundary layer analysis is given in Section 4. Sec. 5 compares the present theory to a simple system of three differential equations for the helium density, the bubble density and the monomer concentration obtained by closing the moment equations for the size distribution according to a simple ansatz introduced in [1]. The last section summarizes our conclusions, and technical details are relegated to Appendices.

2 Nondimensionalization of the kinetic equations

Let $[t]$, $[k]$, $[\tilde{c}]$, $[\rho]$ be typical units of time, cluster size, monomer concentration and cluster density, respectively. Equations (1), (7) and (3) provide the following dominant balances between these scaling units:

$$\frac{[\rho]}{[\tilde{t}]} = 4\pi D [\tilde{c}] a_1 \frac{[k]^{1/3} [\rho]}{[k]}, \quad (8)$$

$$\frac{[\rho] [k]}{[\tilde{t}]} = 4\pi D [\tilde{c}]^2 a_1, \quad (9)$$

$$[k]^2[\rho] = g[\tilde{t}]. \quad (10)$$

To derive these equations, we have assumed that there is a continuum limit with $k \gg 1$ and that the number density of particles in clusters, $\sum_{k=2}^{\infty} k \rho_k$, is much larger than the monomer concentration c . Note that we have three relations (8) - (10) for four unknowns $[\tilde{t}]$, $[k]$, $[\tilde{c}]$, $[\rho]$. In the absence of another relation (for example, a different creation rate $g(\tilde{t}) = G(\tilde{t}/\tau)$, which fixes the time scale $[\tilde{t}] = \tau$), we can express three of these scaling units in terms of the fourth. We find

$$[\tilde{t}] = \frac{[k]^{7/6}}{\sqrt{4\pi Da_1 g}}, \quad [\tilde{c}] = \sqrt{\frac{g}{4\pi Da_1}} [k]^{-1/2}, \quad [\rho] = \sqrt{\frac{g}{4\pi Da_1}} [k]^{-5/6}. \quad (11)$$

We shall now define nondimensional units as

$$\begin{aligned} t = \frac{\tilde{t}}{[\tilde{t}]} &\equiv \kappa^{-7/6} \tilde{t} \sqrt{4\pi Da_1 g}, \\ c = \frac{\tilde{c}}{[\tilde{c}]} &\equiv \kappa^{1/2} \tilde{c} \sqrt{\frac{4\pi Da_1}{g}}, \\ r_k = \frac{\rho_k}{[\rho]} &\equiv \kappa^{5/6} \rho_k \sqrt{\frac{4\pi Da_1}{g}}, \end{aligned} \quad (12)$$

in which we have set $[k] = \kappa$ (any positive number). Equations (1) - (3) and (7) become

$$\frac{dr_k}{dt} = c \kappa^{2/3} [(k-1)^{1/3} r_{k-1} - k^{1/3} r_k], \quad k \geq 3, \quad (13)$$

$$\frac{dr_2}{dt} = 2\kappa c^2 - \kappa^{2/3} 2^{1/3} c r_2, \quad (14)$$

$$\kappa^{-5/3} c + \kappa^{-2} \sum_{k=2}^{\infty} k r_k = t, \quad (15)$$

$$\frac{d}{dt} \sum_{k=2}^{\infty} r_k = 2\kappa c^2. \quad (16)$$

Our nondimensional system of kinetic equations comprises (13) - (15) with $\kappa = 1$ and initial conditions $r_k(0) = 0$, $c(0) = 0$. (16) is a consequence of the previous equations or it can be used instead of (14). Defining an adaptive time $s = \int_0^t c(t') dt'$, we can rewrite our system in the more convenient form:

$$\frac{dr_k}{ds} = (k-1)^{1/3} r_{k-1} - k^{1/3} r_k, \quad k \geq 3, \quad (17)$$

$$\frac{dr_2}{ds} = 2c - 2^{1/3}r_2, \quad (18)$$

$$c + \sum_{k=2}^{\infty} kr_k = t, \quad (19)$$

$$\frac{ds}{dt} = c, \quad (20)$$

with initial conditions $c(0) = r_k(0) = 0$ ($k \geq 2$) and $t(0) = 0$. In order to integrate this system of equations, it is convenient to time differentiate (19) and use (20). The result is

$$c \frac{dc}{ds} + 4c^2 + cM_{1/3} = 1, \quad (21)$$

in which we have defined the moments of the size distribution function $r_k(s)$:

$$M_\mu(s) = \sum_{k=2}^{\infty} k^\mu r_k. \quad (22)$$

M_0 and M_1 are the number densities of bubbles and of helium, respectively. They satisfy:

$$\frac{dM_0}{ds} = 2c, \quad (23)$$

$$\frac{dM_1}{ds} = 4c + M_{1/3}, \quad (24)$$

with zero initial conditions.

The kinetic equations describing formation of helium bubbles are therefore (17), (18), (20), (21) and (22) with zero initial conditions. These equations yield the monomer concentration c and the size distribution function r_k . The number densities of bubbles and of helium are given by (23) and (24).

3 Outer solution and relation to the continuum limit equations

3.1 Continuum limit and similarity solution

A first attempt at approximating the model equations consists of taking the continuum limit of (17) - (20). In fact, assume that

$$r_k(s) = r(k, s), \quad (25)$$

and Taylor expand r in (17) up to first order terms. The result is

$$\frac{\partial r}{\partial s} + \frac{\partial}{\partial k}(k^{1/3}r) = 0, \quad (26)$$

$$\int_0^\infty k r dk = t. \quad (27)$$

We have ignored the monomer concentration in (27). Integrating (26) over $k > 0$, we obtain

$$\frac{d}{ds} \int_0^\infty r dk = \lim_{k \rightarrow 0} (k^{1/3}r),$$

and (23) implies the following signaling condition:

$$\lim_{k \rightarrow 0} (k^{1/3}r) = 2c. \quad (28)$$

The method of characteristics provides the following solution to (26) and (28) with initial condition $c(0) = 0$:

$$r(k, s) = 2k^{-1/3} c(s - a(k)) \theta(s - a(k)), \quad (29)$$

$$a(k) = \frac{3}{2} k^{2/3}, \quad (30)$$

in which $\theta(x) = 1$ if $x > 0$ and $\theta(x) = 0$ if $x < 0$ is the Heaviside unit step function. After a change of variable, the integral condition (27) becomes

$$2 \left(\frac{2}{3} \right)^{3/2} \int_0^s (s - s')^{3/2} c(s') ds' = t, \quad (31)$$

or, equivalently,

$$2 \left(\frac{2}{3} \right)^{1/2} c(s) \int_0^s (s - s')^{1/2} c(s') ds' = 1. \quad (32)$$

The problem (26) - (28) and (31) has a similarity solution whose role will be discussed later. In fact, note that (26) - (28) are invariant under the scaling transformation $r \rightarrow \kappa^{-5/6}r$, $c \rightarrow \kappa^{-1/2}c$, $s \rightarrow \kappa^{2/3}s$, $t \rightarrow \kappa^{7/6}t$, $k \rightarrow \kappa k$, which is suggested by the nondimensionalization (12). Therefore the combinations $\chi =$

$k s^{-3/2}$ and $\rho = s^{5/4} r$ are invariant under the previous scaling transformation. In terms of $\rho = \rho(\chi)$, (26) becomes

$$\frac{d\rho}{ds} = \frac{\rho}{3\chi} \frac{\frac{15}{4}\chi^{2/3} - 1}{\frac{3}{2}\chi^{2/3}}, \quad (33)$$

$$\rho = s^{5/4} r, \quad \chi = k s^{-3/2}. \quad (34)$$

The solution of (33) is

$$r(\chi, s) = \frac{R_0 s^{-5/4} \chi^{-1/3}}{\left(1 - \frac{3}{2} \chi^{2/3}\right)_+^{3/4}}. \quad (35)$$

Here R_0 is a positive constant and $(x)_+ = x \theta(x)$. This similarity solution has integrable singularities at $\chi = 0$ and at $\chi = \chi_0 \equiv (2/3)^{3/2}$ (corresponding to the maximum cluster size $k_f(s)$). Now the signaling condition (28) yields the monomer concentration:

$$c(s) = \frac{1}{2} R_0 s^{-3/4}, \quad (36)$$

and (20) together with $s(0) = 0$ yield the relation between s and the time:

$$s = \left(\frac{7}{8} R_0 t\right)^{4/7}. \quad (37)$$

The constant R_0 is found by inserting (36) in (32), which yields $R_0^2 \sqrt{2/3} B(3/2, 1/4) = 1$, from which,

$$R_0 = \frac{(27\pi)^{1/4}}{\Gamma(1/4)} \approx 0.837042. \quad (38)$$

The self-similar size distribution function has a singularity at its maximum size $\chi = \chi_0$. Fig. 1 shows that this solution is a relatively poor approximation to the numerical solution of the full model. To improve it, we can take into account the effects of discreteness by replacing $1 + 3s^{-1} - 3\chi^{2/3}/2$ instead of $1 - 3\chi^{2/3}/2$ in (35). Then the singularity of the self-similar size distribution function moves closer to the local maximum of the exact numerical solution and the approximation improves, as shown in Figure 2. We observe that the singularity of the self-similar size distribution function occurs before the numerical size distribution function reaches its local maximum, and this effect becomes more noticeable as time increases.

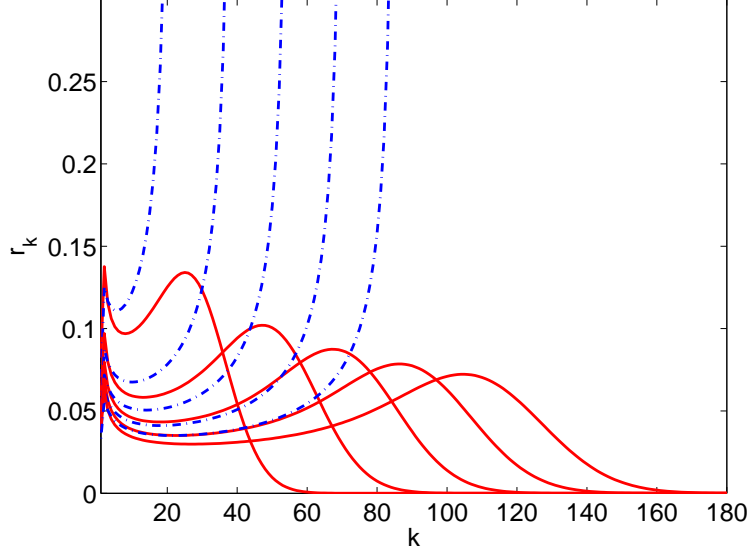


Fig. 1. Nondimensional size distribution function $r_k(t)$ evaluated by solving the full model system of discrete equations (solid line) and the similarity solution (dashed line) at the nondimensional times 100, 200, 300, 400 and 500.

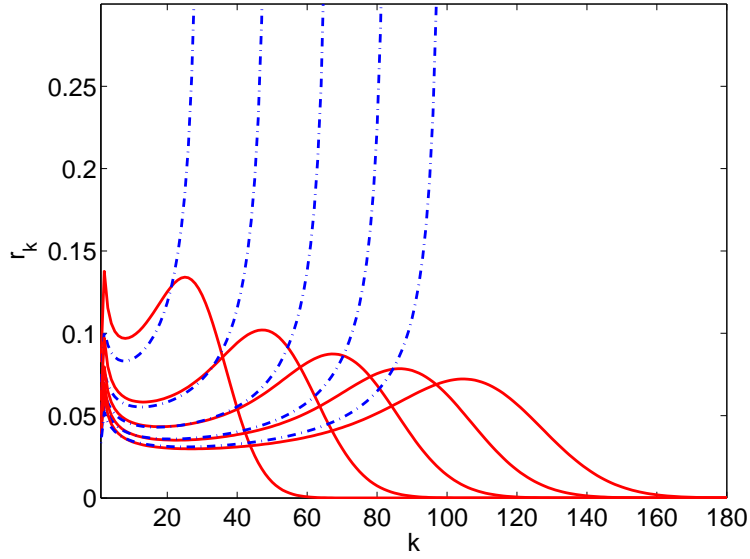


Fig. 2. Same as Fig. 1 but now the dashed line is the similarity solution corrected by replacing $1 + 3s^{-1} - 3\chi^{2/3}/2$ instead of $1 - 3\chi^{2/3}/2$ in (35).

3.2 Outer solution for the discrete problem

The similarity solution of the continuum equations is a poor approximation to the numerical solution of the discrete model. We need to correct it by including the effects of discreteness and by approximating better the equation for the

monomer concentration. The corrections due to discreteness can be found by first solving the linear equations (17) exactly. Laplace transforming (17) and using $r_k(0) = 0$, we obtain

$$\hat{r}_k(\sigma) = \frac{(k-1)^{1/3} \hat{r}_{k-1}}{\sigma + k^{1/3}}, \quad (39)$$

for $k > 2$, from which it follows:

$$k^{1/3} \hat{r}_k(\sigma) = 2 \hat{c}(\sigma) \hat{R}_k(\sigma), \quad (40)$$

$$\hat{R}_k(\sigma) \equiv \prod_{j=2}^k \frac{1}{1 + \sigma j^{-1/3}}, \quad (41)$$

$$r_k(s) = 2k^{-1/3} \int_0^s R_k(s-s') c(s') ds'. \quad (42)$$

These equations give the exact size distribution function in terms of $c(s)$. Inserting (42) in the definition of $M_{1/3}$ and substituting the result in (21), we obtain

$$c \frac{dc}{ds} + 4c^2 + 2c \int_0^s \left[\sum_{k=2}^{\infty} R_k(s-s') \right] c(s') ds' = 1. \quad (43)$$

This integrodifferential equation for c should be solved using the initial condition $c(0) = 0$. Unfortunately, it is not too useful because the integral kernel is written as an infinite series of the inverse Laplace transform of (41), which is rather unwieldy.

To find an approximate form of Eq. (43), we assume that $R_k(s)$ is peaked about its mean value:

$$a(k) \equiv \frac{\int_0^{\infty} s R_k(s) ds}{\int_0^{\infty} R_k(s) ds} = -\frac{\hat{R}'_k(0)}{\hat{R}_k(0)} = \sum_{j=2}^k j^{-1/3}. \quad (44)$$

In Appendix A, we show that

$$a(k) \sim \frac{3}{2} k^{2/3} - 3 + \frac{1}{2 k^{1/3}} \quad (k \rightarrow \infty). \quad (45)$$

We also show that the relative width of the peak in $R_k(s)$, $\sigma/a \sim 2k^{-1/2}/\sqrt{3}$ tends to 0 as $k \rightarrow \infty$. If we assume that $c(s)$ is a smooth function (and this is not always the case), then we may approximate the kernel in the convolution

integral (42) by $R_k(s) \sim \delta(s - a(k))$, so that the size distribution function is given by (29) with $a(k)$ replaced by (45). Note that the first term in the right hand side of (45) coincides exactly with the result (30) obtained by solving the continuum equations (26) and (28). Equation (43) becomes

$$c \frac{dc}{ds} + 4c^2 + 2c \sum_{k=2, a(k) < s} c(s - a(k)) = 1. \quad (46)$$

For large s , the maximum cluster size is such that $a(k_f) \sim 3k_f^{2/3}/2 - 3 = s$. Then we can approximate the sum in (46) by an integral over k from $k = 0$ to $k = k_f(s)$. Changing variables in the integral, (46) becomes

$$c \frac{dc}{ds} + 4c^2 + 2\sqrt{\frac{2}{3}} c \int_0^s (s - s' + 3)^{1/2} c(s') ds' = 1. \quad (47)$$

We would like to compare now the solution of (29), (45), (47) and (20) with zero initial conditions to the numerical solution of the exact discrete model. To this end, it is better to write all unknowns as functions of the time t . Our local theory is then

$$\begin{aligned} r_k(t) &= 2k^{-1/3} c(s(t) - a(k)) \theta(s(t) - a(k)), \\ \frac{dc}{dt} + 4c^2 + 2\sqrt{\frac{2}{3}} c \int_0^t [s(t) - s(t') + 3]^{1/2} [c(s(t'))]^2 dt' &= 1, \\ \frac{ds}{dt} &= c, \\ c(0) = s(0) &= 0. \end{aligned} \quad (48)$$

Figure 3 shows a comparison between the monomer concentration evaluated by solving the full discrete model equations, the local theory (48), the similarity solution and the three moment equations used by Wolfer and coworkers (cf. Section 5 and [1]). In Fig. 3(a), we observe that Wolfer et al's approximation is better for short times, but that the local theory given by (48) provides the best approximation as time goes to infinity, cf. Fig. 3(b). Figure 4 shows the size distribution function calculated at different times by using the local theory (48) (dashed lines) and the numerical solution of the full discrete model. The local theory yields higher cluster densities than the exact solution, a much higher maximum density but it predicts a maximum size which is very close to the local maximum of the real distribution function at large sizes.

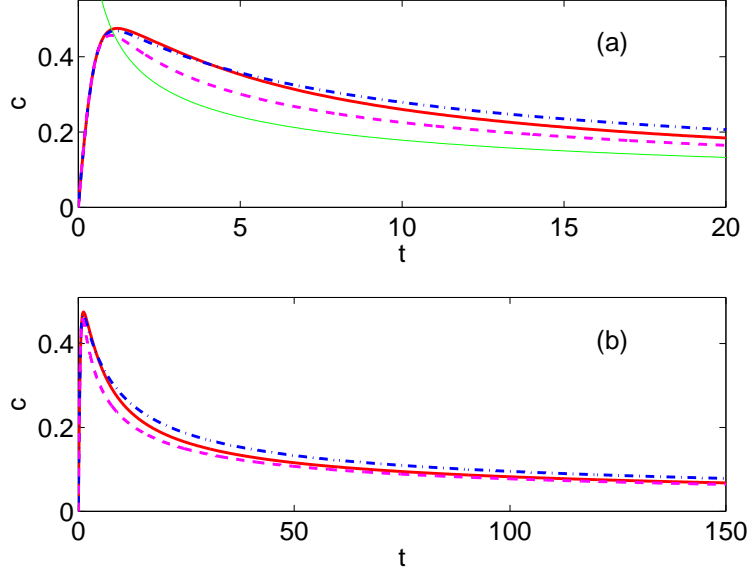


Fig. 3. (a) Monomer concentration $c(t)$ evaluated using: (i) the numerical solution of the discrete equations of the model (solid line), (ii) the local theory (48) (dashed line), (iii) Schaldach and Wolfer's moment equations (dot-dashed line), and (iv) the self-similar solution having a vertical asymptote at $t = 0$ (thin solid line). (b) Same as in (a) for a larger range of times. All variables are written in dimensionless units.

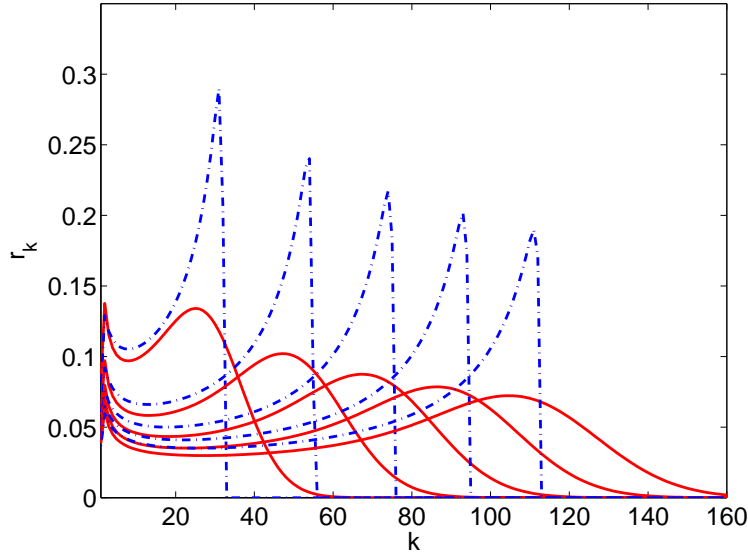


Fig. 4. Dimensionless size distribution function $r_k(t)$ calculated using the numerical solution of the full model discrete equations (solid line) and the local theory (48) (dashed line) at the nondimensional times 100, 200, 300, 400 and 500.

4 Leading edge of the size distribution function

The previous local description of the size distribution function differs substantially from the numerical solution of the model equations for large sizes. However, the maximum of the numerical r_k coincides with the peak of the approximate r_k at $k = k_f(s)$, which is also its leading edge. To improve our asymptotic theory, we should insert a moving boundary layer there. How? We shall use the wave front theory which we introduced in our previous work on homogeneous nucleation [4]. Firstly, let us rewrite (17) and (21) as

$$\frac{d\sigma_k}{ds} = k^{1/3} (\sigma_{k-1} - \sigma_k), \quad k \geq 3, \quad (49)$$

$$\sigma_k = k^{1/3} r_k, \quad (50)$$

$$c \frac{dc}{ds} + 4c^2 + c \sum_{k=2}^{\infty} \sigma_k = 1. \quad (51)$$

Secondly, let us use local coordinates about the inflection point of the wave front leading edge in σ_k , $k = K(s)$, for large k :

$$\sigma_k = S(X, s), \quad X = k - K(s), \quad 1 \ll X \ll K. \quad (52)$$

Substitution of (52) in (49) yields

$$\frac{\partial S}{\partial s} - \frac{\partial S}{\partial X} \frac{dK}{ds} = (K^{1/3} + \frac{1}{3}K^{-2/3}X + \dots) \left(-\frac{\partial S}{\partial X} + \frac{1}{2} \frac{\partial^2 S}{\partial X^2} + \dots \right).$$

Provided

$$\frac{dK}{ds} = K^{1/3}, \quad (53)$$

the distinguished limit of the previous equation for S gives

$$\frac{\partial S}{\partial s} + \frac{1}{3}K^{-2/3}X \frac{\partial S}{\partial X} = \frac{1}{2}K^{1/3} \frac{\partial^2 S}{\partial X^2}. \quad (54)$$

A more detailed derivation using a book-keeping small parameter is included in Appendix B. Note that the inflection point $K(s)$ is different from the local maximum of the distribution function for large sizes, $k_f < K$. If we change variables from the adaptive time s to the front location K , we find an equation in which K scales as X^2 . Thus it is convenient to consider S as a function of the new ‘time’ K and the similarity variable $\xi = X/\sqrt{K}$. Then,

$$K \frac{\partial S}{\partial K} - \frac{\xi}{6} \frac{\partial S}{\partial \xi} = \frac{1}{2} \frac{\partial^2 S}{\partial \xi^2}, \quad (55)$$

$$\xi = \frac{k - K(s)}{\sqrt{K(s)}}. \quad (56)$$

Equation (55) should be solved with boundary condition $S(\infty, K) = 0$ and an appropriate matching condition as $\xi \rightarrow -\infty$.

The solution of (53) is

$$K(s) = \left(\frac{2s}{3} + K_0^{2/3} \right)^{3/2}, \quad (57)$$

in which K_0 is an arbitrary positive constant to be selected later. The solution (28) with $a(k) \sim -3 + 3k^{2/3}/2$ yields the matching condition

$$\sigma_k = 2c \left(s + 3 - \frac{3}{2} k^{2/3} \right)_+ \sim 2c \left(3 - \frac{3}{2} K_0^{2/3} - \xi K^{1/6} \right)_+, \quad (58)$$

in the overlap region: $\sqrt{K} \ll (K - k) \ll K$, as $\xi \rightarrow -\infty$. In Appendix C, we show that the solution of (55) satisfying boundary and matching condition is

$$S(\xi, K) = \frac{2}{\sqrt{6\pi(K^{1/3} - K_0^{1/3})}} \int_0^t [c(t')]^2 e^{-\frac{[\xi K^{1/6} + s(t') - 3 + \frac{3}{2} K_0^{2/3}]^2}{6(K^{1/3} - K_0^{1/3})}} dt'. \quad (59)$$

Clearly, the front solution (59) contributes to the moment $M_{1/3}$ in (21) for small times corresponding to k in the overlap region. Since S is matched to a variable outer solution, it is convenient to pick a time $t_p(t)$ corresponding to k in the overlap region to split the time interval $(0, t)$ in (48) into two subintervals. For $0 < t' < t_p(t)$, we use the front approximation (50), (52) and (59) whereas we use the outer approximation (28) with (45) for times in $(t_p(t), t)$. The patching time solves

$$s(t_p) = \xi_p [K(s(t))]^{1/6} + 3 - \frac{3}{2} K_0^{2/3}, \quad (60)$$

for ξ_p in the overlap region. Since the width of the gaussian in (59) is $\sqrt{6}$, we may choose $\xi_p \geq \sqrt{6}$. Up to the patching time, the contribution of the leading edge (59) to the moment $M_{1/3}$ in (21) is $\int_{-\infty}^{\infty} S(\xi, K) K^{1/2} d\xi = 2 K^{1/3} \int_0^{t_p} [c(t')]^2 dt'$. Taking into account the approximation (28), we obtain

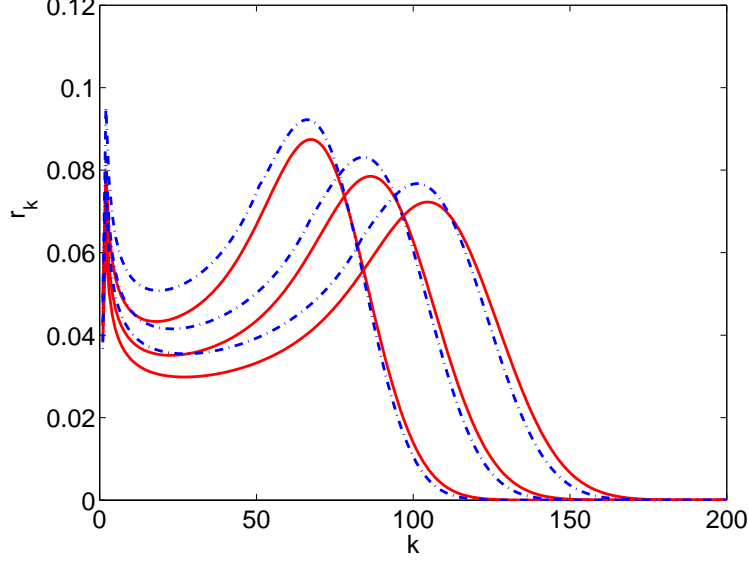


Fig. 5. Nondimensional size distribution function $r_k(t)$ evaluated using the composite solution (61) - (62) (dashed line) and the numerical solution of the full model discrete equations (solid line) at the nondimensional times 300, 400 and 500.

$$\begin{aligned} \frac{dc}{dt} + 4c^2 + 2\sqrt{\frac{2}{3}}c \int_{t_p(t)}^t [s(t) - s(t') + 3]^{1/2} [c(t')]^2 dt' \\ + 2[K(s(t))]^{1/3} c \int_0^{t_p(t)} [c(t')]^2 dt' = 1. \end{aligned} \quad (61)$$

Fig. 5 compares the numerical solution of the full discrete model equations to the composite solution:

$$\begin{aligned} r_k = 2k^{-1/3}c(s(t) - a(k))_+ \theta(K - \xi_p \sqrt{K} - k) \\ + \frac{2\theta(k - K + \xi_p \sqrt{K})}{\sqrt{6\pi(K^{1/3} - K_0^{1/3})}} \int_0^t [c(t')]^2 e^{-\frac{[\xi K^{1/6} + s(t') - 3 + \frac{3}{2}K_0^{2/3}]^2}{6(K^{1/3} - K_0^{1/3})}} dt', \end{aligned} \quad (62)$$

plus (61) for the monomer concentration. We have used the numerical values $K_0 = 0.5$ and $\xi_p = \sqrt{6}$ without looking for an optimal fit to the numerical solution of the full model equations by varying K_0 and ξ_p . The agreement between our theory and the numerical solution of the full model is much better than that achieved by using only the outer solution. Although our effective small parameter is the reciprocal of the wave front location (and $1/K \rightarrow 0$ as $t \rightarrow \infty$), the poor agreement between the outer solution and the numerical solution at large sizes precludes a better agreement between the composite solution and the numerical solution.

5 Moment closure

The composite solution is computationally costly if all we want to calculate is the monomer concentration because we need to calculate $K(s(t))$, $t_{p(t)}$ and $c(s - a(k))$ at each instant of time. A different approximation involving only equations that are local in time was used by Schaldach and Wolfer [1] to approximate the number densities of monomers, bubbles and helium. Note that Equations (21), (23) and (24) would form a closed system of equations if we could express $M_{1/3}$ in terms of M_0 and M_1 . Physically speaking, $M_{1/3}/M_0$ and M_1/M_0 have the meaning of average bubble radius and average helium density. If we impose

$$\frac{M_1}{M_0} \approx \frac{4\pi}{3} \left(\frac{M_{1/3}}{M_0} \right)^3 \implies M_{1/3} \approx \left(\frac{3}{4\pi} \right)^{1/3} M_1^{1/3} M_0^{2/3}, \quad (63)$$

we obtain the following closed system of three differential equations [1]

$$\frac{dM_0}{ds} = 2c, \quad (64)$$

$$\frac{dM_1}{ds} = 4c + \left(\frac{3}{4\pi} \right)^{1/3} M_1^{1/3} M_0^{2/3}, \quad (65)$$

$$c \frac{dc}{ds} + 4c^2 + \left(\frac{3}{4\pi} \right)^{1/3} c M_1^{1/3} M_0^{2/3} = 1, \quad (66)$$

plus Eq. (20) relating s and the time. For long times, these equations possess the same scaling symmetry as the continuum equations and their solutions tend to a similarity solution for long times. A different closure assumption can be obtained by combining the idea of preserving the scaling symmetry with a closure assumption related to (63), as explained in Appendix D. The resulting moment equations have solutions which become self-similar for appropriate intervals of time, but these solutions approximate the numerical solution of the kinetic equation less well than those of (64) - (66).

Figure 6 shows a comparison between the size distribution function (29) and (45) calculated with the monomer concentration resulting from the moment equations (64) - (66) and the numerical solution of the full model. We observe that the maximum at large sizes is predicted to occur at much larger sizes. Thus the moment equations provide a worse prediction than the outer solution (48), and, of course, worse than the composite solution (61) - (62).

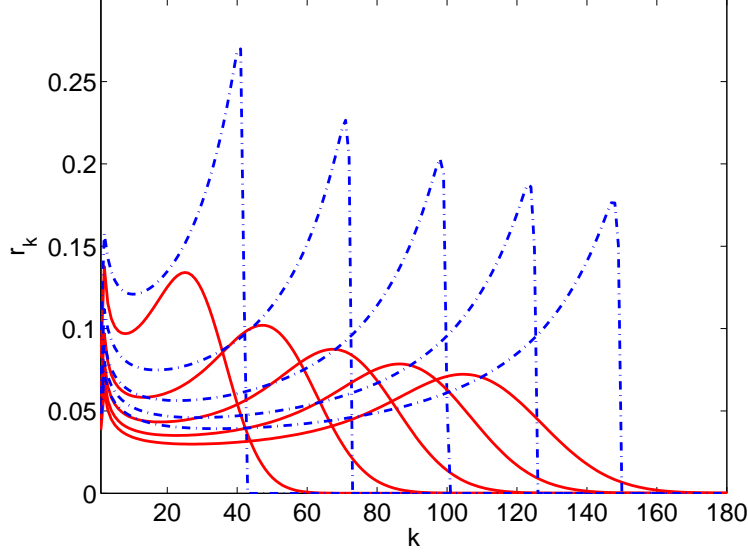


Fig. 6. Nondimensional size distribution function $r_k(t)$ of (29) and (45) with monomer concentration given by the moment equations (64) - (66) (dashed line) and the numerical solution of the full model discrete equations (solid line). Times are as in Fig. 3.

6 Conclusions

In Section 3, we have found the composite solution (61) - (62) to the discrete kinetic equations. The outer approximation is a solution of the continuum limit of the discrete equations corrected by the effects of discreteness. The inner approximation follows from a wave front expansion previously introduced for transient homogeneous nucleation [4]. A similar equation for the wave front profile was obtained by King and Wattis in the case of the Becker-Döring equations with rate constants having a power law dependence on cluster size [5]. While in the case of nucleation the outer approximation was a simple constant profile in the wake of the wave front, in the present case of growing helium bubbles, the outer approximation is a time and size dependent function depending on the monomer concentration. The monomer concentration satisfies an integrodifferential equation comprising contributions of both the outer and the inner solutions. As time increases, the outer solution tries to achieve a self-similar form in the variable $\chi = k/s^{3/2}$ corrected by discreteness effects, as suggested by Fig. 2. The inner solution is determined by the position of the wave front $K(s(t))$ and by the similarity variable $\xi = (k - K)/\sqrt{K}$, which is different from χ . Inner and outer solution have an overlap domain $1 \ll \sqrt{K} \ll (K - k) \ll K$ and are patched at a point thereof to yield the composite solution.

We have also compared our approximations to Schaldach and Wolfer's mo-

ment closure of Section 5 supplemented with the formulas (29) and (45) for the size distribution function. Fig. 3 shows that the similarity solution for $c(t)$ is consistently above the numerical solution of the model, while the moment closure solution is consistently below. Then the maximum of the size distribution function approximated using the similarity solution (resp. the moment closure theory) occurs before (resp. after) the real maximum. In contrast with these approximations, the outer solution (48) yields a better match to the monomer concentration for large times and to the location of the maximum of the size distribution function. Corrected with the boundary layer formula, the composite solution (61) - (62) gives the best match to the numerical solution of all the approximations described in this paper.

Acknowledgements

This work has been supported by the Spanish MEC grant MAT2005-05730-C02, and by the US NSF grant 0515616.

This work was performed under the auspices of the U.S. Department of Energy by University of California, Lawrence Livermore National Laboratory under contract W-7405-Eng-48.

A Approximating the sums $\sum_{j=2}^k j^{-\alpha}$.

For $0 < \alpha < 1$ and $k \rightarrow \infty$, these expressions are Riemann sums whose j th term equals the area under a rectangle of height $(j-1)^{-\alpha}$ and basis 1. These Riemann sums can be approximated by the integral minus the sum of the areas of triangles of height $[(j-1)^{-\alpha} - j^{-\alpha}]$ and basis 1. We thus have

$$\sum_{j=2}^k j^{-\alpha} = \sum_{j=1}^k j^{-\alpha} - 1 \approx k^{1-\alpha} \int_{1/k}^1 \frac{dx}{x^\alpha} + \frac{1}{2} \sum_{j=2}^k [j^{-\alpha} - (j-1)^{-\alpha}] - 1,$$

and therefore

$$\sum_{j=2}^k j^{-\alpha} \approx \frac{k^{1-\alpha}}{1-\alpha} - \frac{5-3\alpha}{2(1-\alpha)} + \frac{1}{2k^\alpha}.$$

The function $a(k)$ is given by the sum with exponent $1/3$, which yields (45). Similarly, the half-width of the peak is given by $\sigma(k)$,

$$\begin{aligned} \sigma(k)^2 &\equiv \int_0^\infty [s - a(k)]^2 R_k(s) ds = \hat{R}''(0) - [\hat{R}'(0)]^2 = \sum_{j=2}^k j^{-2/3} \\ &\sim 3k^{1/3} - \frac{9}{2} + \frac{1}{2k^{2/3}} \quad (k \rightarrow \infty). \end{aligned}$$

As explained in the text, the relative width of the peak of $R_k(s)$, $\sigma/a \sim 2k^{-1/2}/\sqrt{3}$ tends to 0 as $k \rightarrow \infty$.

B Derivation of the equation for the wave front profile using a book-keeping small parameter.

Let us insert

$$\sigma_k = S(X^*, s^*), \quad X^* = \epsilon^\gamma \left(k - \frac{K^*(s^*)}{\epsilon} \right), \quad s^* = \epsilon^{2/3} s, \quad \epsilon \rightarrow 0+,$$

in (49) instead of (52). The small parameter ϵ represents location of the wave front at a typical large size. We find

$$\begin{aligned} \epsilon^{2/3} \frac{\partial S}{\partial s^*} - \epsilon^{\gamma-1/3} \frac{\partial S}{\partial X^*} \frac{dK^*}{ds^*} &= \left(\frac{(K^*)^{1/3}}{\epsilon^{1/3}} + \frac{\epsilon^{2/3-\gamma}}{3} (K^*)^{-2/3} X^* + \dots \right) \\ &\quad \times \left(-\epsilon^\gamma \frac{\partial S}{\partial X^*} + \frac{\epsilon^{2\gamma}}{2} \frac{\partial^2 S}{\partial (X^*)^2} + \dots \right), \end{aligned}$$

from which

$$\begin{aligned} \epsilon^{2/3} \left(\frac{\partial S}{\partial s^*} + \frac{X^*}{3(K^*)^{2/3}} \frac{\partial S}{\partial X^*} \right) + \epsilon^{\gamma-1/3} \frac{\partial S}{\partial X^*} \left((K^*)^{1/3} - \frac{dK^*}{ds^*} \right) &= \\ \frac{\epsilon^{2\gamma-1/3} (K^*)^{1/3}}{2} \frac{\partial^2 S}{\partial (X^*)^2} + \dots \end{aligned}$$

Provided

$$\frac{dK^*}{ds^*} = (K^*)^{1/3},$$

and $\gamma = 1/2$, we find the equation

$$\frac{\partial S}{\partial s^*} + \frac{X^*}{3(K^*)^{2/3}} \frac{\partial S}{\partial X^*} = \frac{(K^*)^{1/3}}{2} \frac{\partial^2 S}{\partial (X^*)^2},$$

in the limit as $\epsilon \rightarrow 0+$. The previous two equations are (53) and (54) once we revert to the variables s and K .

C Solution of the equation for the leading front

Defining $J = -\partial S/\partial \xi$, we find the following equation for J :

$$K \frac{\partial J}{\partial K} - \frac{1}{6} \frac{\partial(\xi J)}{\partial \xi} = \frac{1}{2} \frac{\partial^2 J}{\partial \xi^2}.$$

The Fourier transform of $J(\xi, \cdot)$ satisfies the hyperbolic equation

$$K \frac{\partial \hat{J}}{\partial K} + \frac{\eta}{6} \frac{\partial \hat{J}}{\partial \eta} = -\frac{\eta^2}{2} \hat{J},$$

which is readily solved by the method of characteristics in terms of an arbitrary initial condition $\hat{J}_0(\eta_0)$. Inverting the Fourier transform and going back to the function S , we obtain

$$S(\xi, K) = \mathcal{S}(K) + \frac{1}{\sqrt{6\pi[1 - (K_0/K)^{1/3}]}} \int_{-\infty}^{\infty} S_0(\xi_0) \exp \left[-\frac{(\xi - \xi_0)^2}{6[1 - (K_0/K)^{1/3}]} \right] d\xi_0,$$

in which $\mathcal{S}(K)$ and $S_0(\xi_0)$ are both arbitrary. As $\xi \rightarrow -\infty$, the integral can be approximated by the Laplace method with the result $S(\xi, K) \sim \mathcal{S}(K) + S_0(\xi)$. The matching condition (58) gives $S_0 \sim 2c(3 - K^{1/6}\xi - 3K_0^{2/3}/2) - \mathcal{S}(K)$, thereby yielding

$$S(\xi, K) = \frac{2}{\sqrt{6\pi[1 - (K_0/K)^{1/3}]}} \int c \left(K^{1/6}\xi_1 + 3 - \frac{3K_0^{2/3}}{2} \right) e^{-\frac{(\xi+\xi_1)^2}{6[1-(K_0/K)^{1/3}]}} d\xi_1.$$

Changing variables from ξ_1 to $s' = K^{1/6}\xi_1 + 3 - 3K_0^{2/3}/2$, we find

$$S(\xi, K) = \frac{2}{\sqrt{6\pi(K^{1/3} - K_0^{1/3})}} \int_0^s c(s') e^{-\frac{\left(K^{1/6}\xi - 3 + \frac{3K_0^{2/3}}{2} + s'\right)^2}{6(K^{1/3} - K_0^{1/3})}} ds'. \quad (\text{C.1})$$

The ends of the integration interval in this expression are set to 0 and s because those are the extremes of the interval over which the monomer concentration exists. Changing variables in this formula from s' to the time t' , we obtain (59).

The width of the Gaussian in (C.1) is $\sqrt{6}$. Thus a typical point in the overlap region is $k_p = K - \xi_p \sqrt{K}$ with $\xi_p \geq \sqrt{6}$. The corresponding adaptive time is

$$s_p = s + 3 - \frac{3}{2}k_p^{2/3} \sim \xi_p[K(s)]^{1/6} + 3 - \frac{3}{2}K_0^{2/3},$$

and the corresponding time is given by (60).

D Moment equations following from a closure assumption preserving scaling symmetry

Let us assume that the size distribution function has the scaling form

$$r_k(s) = \frac{M_0(s)^2 l_1}{M_1(s) l_0^2} \tilde{r}(x), \quad (\text{D.1})$$

$$x = \frac{M_0(s) l_1}{M_1(s) l_0} k, \quad (\text{D.2})$$

$$l_\mu = \int_0^\infty x^\mu \tilde{r}(x) dx. \quad (\text{D.3})$$

The definition (22) of the moments together with (D.1) - (D.3) imply

$$M_\mu = \frac{l_\mu}{l_1^\mu l_0^{1-\mu}} M_1^\mu M_0^{1-\mu}. \quad (\text{D.4})$$

We can use (D.4) for $\mu = 1/3$ to close the system of equations (21), (23) and (24), with the result

$$\frac{dM_0}{ds} = 2c, \quad (\text{D.5})$$

$$\frac{dM_1}{ds} = 4c + \lambda M_1^{1/3} M_0^{2/3}, \quad (\text{D.6})$$

$$c \frac{dc}{ds} + 4c^2 + \lambda c M_1^{1/3} M_0^{2/3} = 1, \quad (\text{D.7})$$

$$\frac{ds}{dt} = c, \quad (\text{D.8})$$

$$\lambda = \frac{l_{1/3}}{l_1^{1/3} l_0^{2/3}}. \quad (\text{D.9})$$

These equations become (64) - (66) if $\lambda = (4\pi/3)^{-1/3}$. To make them compatible with the previously found similarity solution, we consider the reduced system given by (D.5) and the approximate equations

$$\frac{dM_1}{ds} = \lambda M_1^{1/3} M_0^{2/3} = \frac{1}{c}, \quad (\text{D.10})$$

which have the same scaling symmetry as in the case of the continuum limit. Thus they have the similarity solution

$$c = C_1 s^{-3/4}, \quad (\text{D.11})$$

for a certain constant C_1 . From (D.5) and (D.10) (written as $dM_1/ds = 1/c$), we obtain

$$M_0 = 8 C_1 s^{1/4}, \quad M_1 = \frac{4 s^{7/4}}{7 C_1}, \quad (\text{D.12})$$

whereby (D.10) yields

$$C_1 = \frac{7^{1/4}}{4} \lambda^{-3/4}. \quad (\text{D.13})$$

We shall now use Eq. (35) for r_k and (D.1) and (D.11) - (D.13) to find \tilde{r} . Straightforward but lengthy calculations yield

$$\tilde{r}(x) = \frac{l_0}{6 x_M} \left(\frac{x}{x_M} \right)^{-1/3} \left[1 - \left(\frac{x}{x_M} \right)^{2/3} \right]_+^{-3/4}, \quad (\text{D.14})$$

$$x_M = \left(\frac{7 l_1}{6 l_{1/3}} \right)^{3/2}. \quad (\text{D.15})$$

With this reduced size distribution function we can check that (D.3) becomes $l_0 = l_0$ for $\mu = 0$ whereas it becomes

$$l_1 = \sqrt{\frac{7 l_1^3}{3 \pi l_{1/3}^3}} \frac{l_0 \Gamma(1/4)^2}{12}, \quad (\text{D.16})$$

$$l_{1/3} = \sqrt{\frac{3 l_{1/3}}{7 \pi l_1}} \frac{l_0 \Gamma(1/4)^2}{6}, \quad (\text{D.17})$$

for $\mu = 1$ and $1/3$, respectively. These two last equations and (D.15) imply that

$$l_{1/3} = \frac{7}{6} l_1, \quad x_M = 1. \quad (\text{D.18})$$

Thus (D.18) are required for the reduced size distribution function to be consistent with the definitions of the l_μ . Using (D.16) - (D.18) in (D.9) and (D.13),

it is possible to show that $C_1 = R_0/2$ given by (38) and we get the same similarity solution as before.

Had we used Schaldach and Wolfer's closure $\lambda = (4\pi/3)^{-1/3}$, we would have obtained the following similarity solution to the reduced system (D.5) and (D.10):

$$c = C_2 s^{-3/4}, \quad M_0 = 4 C_2 s^{1/4}, \quad M_1 = \frac{4}{7 C_2} s^{7/4}, \quad C_2 = \frac{1}{2} \left(\frac{7\pi}{3} \right)^{1/4} \quad (\text{D.19})$$

If we employ time instead of the variable s , (D.19) becomes

$$c = \left(\frac{4\pi}{3} \right)^{1/7} 7^{-2/7} t^{-3/7}, \quad M_0 = \left(\frac{4\pi}{3} \right)^{2/7} 7^{3/7} t^{1/7}, \quad M_1 = t. \quad (\text{D.20})$$

References

- [1] Schaldach, C. M., Wolfer, W. G., 2004. Kinetics of Helium bubble formation in nuclear and structural materials, in *Effects of Radiation on Materials: 21st Symposium*. M. L. Grossbeck; T. R. Allen; R. G. Lott; A. S. Kumar, eds. ASTM STP 1447, ASTM International, West Conshohocken.
- [2] Schwartz, A. J., Wall, M. A., Zocco, T. G., Wolfer, W. G., 2005. Characterization and modelling of helium bubbles in self-irradiated plutonium alloys. *Phil. Mag.* **85**, 479-488.
- [3] McKendrick, A. G., 1914. Studies on the theory of continuous probabilities, with special reference to its bearing on natural phenomena of a progressive nature. *Proc. London Math. Soc.* **13**, 401-416.
- [4] Neu, J. C., Bonilla, L. L., Carpio, A., 2005. Igniting homogeneous nucleation. *Phys. Rev. E* **71**, 021601 (14 pages).
- [5] King, J.R., Wattis, J.A.D., 2002. Asymptotic solutions of the Becker-Döring equations with size-dependent rate constants. *J. Phys. A* **35**, 1357-1380.